Spatial measurements of moving space-charge domains in *p*-type ultrapure germanium

A. M. Kahn, D. J. Mar, and R. M. Westervelt
Department of Physics and Division of Applied Sciences, Harvard University, Cambridge, Massachusetts 02138
(Received 18 October 1990)

We use a moveable capacitive probe to study experimentally the spatially dependent voltage, electric field, and charge density associated with a periodic current instability in voltage-biased ultrapure *p*-type Ge at 4.2 K. The data show that each period of oscillation is associated with the movement of a high-field space-charge domain along the conduction direction. The domains are 2 mm wide, ~ 3 V/cm in amplitude, and move at a velocity of approximately 1200 cm/s. The onset of the instability for increasing bias field is characterized by nonperiodic current spikes, which are due to the nucleation and movement of solitary domains across the sample. We have also succeeded in nucleating a solitary domain when the sample is biased below the threshold for spontaneous current instability by applying a brief upward pulse in the applied field.

I. INTRODUCTION

Spontaneous current instabilities have been observed in a number of semiconductors at low temperatures including Ge,[1-5] GaAs,[6] and InSb.[7] For increasing bias, these systems exhibit a transition from time-independent dc current flow to either periodic or chaotic current oscillations.[8] While these systems have been carefully studied in the temporal regime, less work has been done on the corresponding spatial structures. One exception is the work of Mayer *et al.*, who have used low-temperature scanning electron microscopy to examine current filaments in Ge (Ref. 9) and GaAs.[10]

A periodic current oscillation has been observed in ultrapure *p*-type Ge for a range of bias voltages beyond the threshold for impurity breakdown. This is a spatially extended experimental system that exhibits frequency locking and a transition to a chaotic temporal oscillation. Gwinn and Westervelt used this system to verify the universality of the frequency-locking transition[5] to chaos and the $f(\alpha)$ spectrum[11] at the critical line. In this paper we use a moveable capacitive probe, similar to that used by Gunn,[12] to study the spatial variation of the electric field associated with the periodic current instability in the absence of ac drive. We show that each period of the current oscillation is associated with the nucleation and subsequent movement of a solitary high-field domain. The onset of the periodic oscillation occurs via an unusual route, in which the spatially extended nature of the system seems to play a crucial role. The spectral purity of the oscillation (≈ 80 dB), and the convenient length scale (mm) and frequency range (kHz) make this a useful system for the experimental study of spatiotemporal dynamics. The domains travel through the samples as noninteracting solitary waves, but there is a global feedback mechanism, because the spatial integral of the electric field is fixed by the dc voltage bias.

The paper is organized as follows. Section II of this paper describes the sample properties and discusses the Ohmic contacts. The experimental method used to take spatial measurements of the oscillating local voltage is described in Sec. III. Section IV describes the basic current-voltage characteristics of the sample as well as temporal measurements of the current instability. Because the onset of the spontaneous oscillation for increasing voltage bias is unusual, this transition is examined in some detail. Section V shows the results of using the capacitive probe to determine the spatially dependent electric field when the sample is dc biased in the oscillating regime. In Sec. VI we examine the response of the sample to a step and to a pulse in the applied bias.

II. SAMPLES AND CONTACTS

The samples used in this work are undislocated *p*-type ultrapure Ge grown at Lawrence Berkeley Laboratory;[13] they were cut from the same crystal as those used for earlier work on the quasiperiodic transition to chaos.[5,11] The total acceptor concentration $N_A \sim 2\times 10^{11}$ cm^{-3} consists primarily of divacancy hydrogen (DVH) complexes[13] which form an acceptor level 72 meV above the valence band. At liquid-He temperatures, these relatively deep levels are frozen out and the carrier concentration is determined by the underlying residual shallow acceptors, predominantly B with concentration $\sim 1\times 10^{11}$ cm^{-3} and binding energy 10 meV. The samples are appreciably compensated. We have found qualitatively and quantitatively similar oscillations in other crystals[14] of ultrapure Ge which contain only shallow acceptor levels, evidence that the DVH levels are not active in the dynamics at liquid-He temperatures. The cross section for impact ionization of holes by DVH levels is far smaller than for shallow acceptors due to their higher binding energy, and they are expected to play no role in the dynamics of domain motion on the millisecond time scales studied here.

Samples were cut to dimensions $4.0\times 4.0\times 14.5$ mm^3 and B ion-implanted contacts were fabricated on opposite 4×4 mm^2 faces, with the $\langle 100\rangle$ axis along the conduction direction. We chose this geometry to ensure that all

electric field lines lie along the length of the sample. After cutting to size the sample was etched in 6:1 HNO_3:HF by volume and quenched in methanol to remove surface damage and minimize surface traps. Making electrical contacts to Ge which are Ohmic at liquid-He temperatures is difficult, due to the difference in work functions. Holes flow from the Ge into the contact and the Ge bands bend downward in order to align the Fermi levels, producing a Schottky barrier. The current density at the contact is limited by the rate of thermionic emission[15] across the barrier,

$$J = BT^2 \exp(-e\Phi_b / k_B T) , \quad (1)$$

where $B = 41$ A/cm^2 K^2 is Richardson's constant for holes in Ge, T is the temperature, e is the electronic charge, Φ_b is the barrier height, and k_B is Boltzmann's constant. The resulting current density through a metal-Ge contact would be very small since for most metals $e\Phi_b \gg k_B T$ at liquid-He temperatures. Ohmic contacts are obtained using B ion implantation to degenerately dope a thin layer of Ge between the ultrapure semiconductor and the metal contact. This has been shown experimentally to result in a much smaller barrier,[16] resulting in Ohmic contacts. If care is not taken to obtain Ohmic contacts, current filaments may form between the contacts similar to the arcing that occurs in a gas between two capacitor plates at sufficiently high voltages. To test for the presence of current filaments in our samples we prepared a sample with one of the contacts divided into four separate regions. Upon simultaneously monitoring the current through each of these regions, we found roughly equal current densities for all bias voltages, even when the current was oscillating.[14] Had there been current filaments in our sample we would expect the current through one of the four regions to have been much larger than the others.

III. EXPERIMENTAL SETUP

In order to measure the spatial dependence of the sample voltage, we use a moveable capacitive probe, made from a Be-Cu wire 130 μm in diameter. The probe wire is carefully shielded to minimize any stray pickup. A thin (50 μm) sheet of mica is laid across the top of the sample to provide a smooth surface on which the wire can move and to prevent the wire from mechanically stressing the sample. The wire is laid across the sample width and perpendicular to the conduction direction, in contact with the mica. This measurement geometry assumes the absence of transverse electric fields, which has been experimentally verified by moving a probe with a very fine tip along the surface of the sample transverse to the current direction. In the postbreakdown region in which these measurements are taken, the carrier concentration is $p \sim 10^{10}$ cm^{-3}, and the dielectric screening length perpendicular to the conduction direction is smaller than the probe diameter. Thus the probe senses the potential only near the surface of the sample. Numerical calculations show that the longitudinal spatial dependence of the capacitive coupling of the probe to the sample is approximately Lorentzian, with a full width at half maximum of one wire diameter; we estimate that the actual spatial resolution is of this order. The probe is mounted inside the Dewar on a translation stage which is controlled via a mechanical feedthrough. For all measurements reported here the sample temperature is maintained at 4.2 K and the sample is surrounded by a radiation shield at the same temperature.

A block diagram of the experimental setup used to take spatial measurements of the sample voltage with dc bias is shown in Fig. 1. A dc voltage is applied across the sample in series with series resistor R (10 Ω), chosen so that $R \ll R_s$, where R_s is the sample resistance. The probe couples to the sample with capacitance $C_p \approx 0.2$ pF. The current induced in the probe by the local time-dependent voltage is integrated using a charge-coupled amplifier consisting of a low-noise field-effect transistor (FET)-input op amp and a feedback capacitor C_f (2 pF). The output of this amplifier V_{out} is proportional to the local sample voltage: $V_{\text{out}} = -(C_p / C_f) V_s$. We record the time-varying voltage V_{out} at 59 sequential positions separated by 0.25 mm using a transient digitizer at a sampling rate of 256 kHz. These time series are synchronized by triggering the digitizer on a fixed phase of the sample current, which is measured by amplifying the voltage across the small series resistor R. The recorded signals are then normalized with respect to variations in the coupling capacitance C_p along the sample length. The spatial voltage profile of the sample is reconstructed by plotting the voltage at successive times during one period of the current oscillation. To obtain the corresponding spatial profiles of electric field ($E = -\partial V / \partial x$) and space-charge density ($\rho \propto -\partial^2 V / \partial x^2$) we pass the data through first- and second-derivative digital filters with high-spatial-frequency rolloffs.[17]

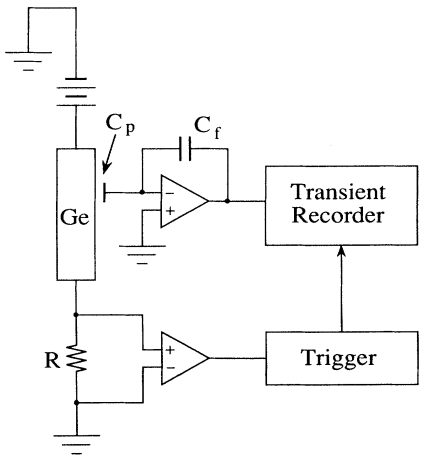

FIG. 1. Schematic diagram of the circuit used to measure the local sample voltage, with pickup capacitance $C_p \approx 0.2$ pF, feedback capacitance $C_f = 2$ pF, and series resistance $R = 10$ Ω.

IV. TWO-TERMINAL MEASUREMENTS

A log-log plot of the time-averaged current as a function of applied dc electric field E_{dc} (voltage/sample length) is shown in Fig. 2. For $E_{dc} < 0.1$ V/cm the hole mobility and concentration do not vary with the applied field, resulting in a linear field dependence of the current. For larger electric fields the current increases superlinearly with field as the hole lifetime increases.[18] When the rate of impact ionization equals the rate of hole recombination, the current increases sharply at a characteristic breakdown field.

Figure 3 shows the time-averaged current as a function of applied electric field, plotted with linear axes. As expected, the *I-V* curves for the two polarities, labeled "A positive" and "B positive," are quite similar. As shown, beyond the breakdown field both *I-V* curves flatten out and the curve with *A* positive has a region of negative slope. Several authors[19,20] have suggested that beyond breakdown there may be a region of negative differential resistance (NDR) in the plot of local current density as a function of local electric field. Teitsworth[19] has used a rate-equation model to show that a region of NDR can occur in extrinsic photoconductors due to the combined effects of velocity saturation of free carriers and negative field dependence in the rate of impact ionization. Mitin[20] has used a Fourier analysis of the Boltzmann transport equation to show that ionized impurity scattering and velocity saturation with the concomitant optical-phonon emission can result in NDR in compensated semiconductors at low temperatures. It is well known that voltage-biased bulk semiconductors with *n*-shaped

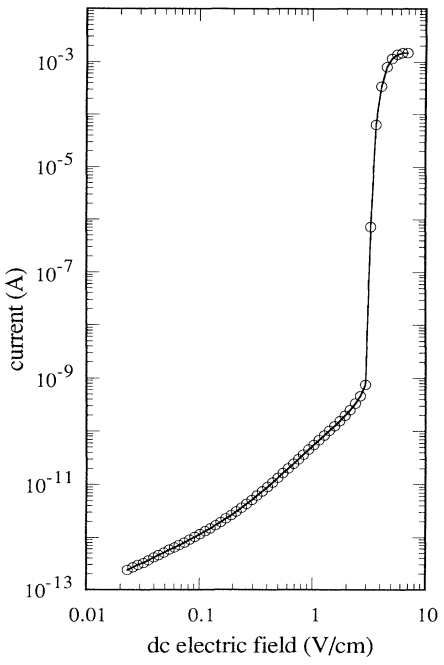

FIG. 2. Current vs applied bias field. The line is drawn as a guide.

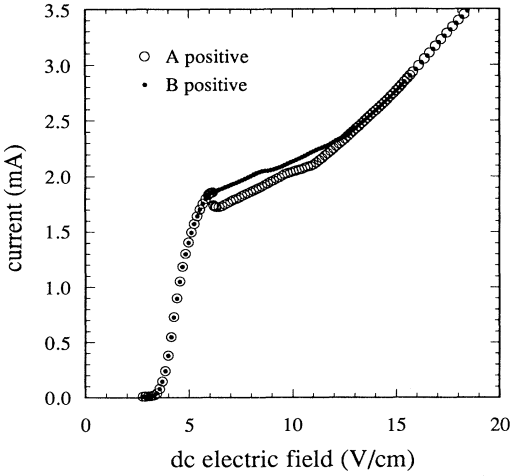

FIG. 3. Time-averaged current vs applied bias field for both polarities, labeled "A positive" and "B positive."

NDR may be unstable to the formation of space-charge domains,[21] as in GaAs Gunn diodes. These space-charge domains typically move through the semiconductor, resulting in current oscillations at a frequency equal to the inverse of the domain transit time. Recently, Bonilla and Teitsworth[22] have used the difference in time scales between dielectric relaxation and the much slower carrier population dynamics to allow a phase plane analysis of the rate-equation model of Ref. 19. Bonilla and Teitsworth show that for an infinitely long sample with current bias there exists a homoclinic orbit in the phase plane corresponding to a solitary traveling domain.

For $E_{dc} > 6.1$ V/cm current oscillations are observed for both polarities of voltage bias, but the oscillation with A positive is cleaner and larger than that with the reverse polarity. This asymmetry may be due to slight differences between the implanted contacts, since the same asymmetry was observed in other samples which were implanted simultaneously. In this paper we focus on the observed instability with contact A positive and all remaining data are given for this polarity.

The instability first appears at a bias of $E_{dc} = 6.160$ V/cm as a small, noisy current oscillation with a fundamental frequency of approximately 6 kHz. When the bias is increased slightly, large negative current spikes occur at long irregular intervals in addition to the small, 6-kHz oscillation. Figure 4 shows six successive time traces of the sample current as E_{dc} is increased from 6.180 V/cm to 6.276 V/cm. The time trace in Fig. 4(a) shows two spikes 19 ms apart. Following each spike the amplitude of the small, 6-kHz oscillation decreases by a factor of 10; over the next several milliseconds the amplitude of the 6-kHz oscillation returns to its previous level as shown. After a variable time interval another downward-current spike occurs. As the bias is increased the average interval between spikes decreases. Figure 4(b) shows six spikes occurring over the same time span as in Fig. 4(a). When the applied dc bias is further increased, one spike often seems to nucleate another, result-

ing in groups of two or more connected spikes. In Fig. 4(c) with $E_{dc}=6.214$ V/cm, there are 15 spikes, including two pairs of spikes. At this bias the small, 6-kHz oscillation resumes immediately following most spikes, as opposed to the gradual growth observed in Fig. 4(a). The time trace in Fig. 4(d), taken with $E_{dc}=6.235$ V/cm, shows groups of two, three, and four spikes, with brief intervals between groups. In Fig. 4(e), with $E_{dc}=6.249$ V/cm, longer groups of spikes are observed. The height of the individual spikes in most cases alternates between smaller and larger spikes. When the bias is increased to $E_{dc}=6.255$ V/cm, the delay between groups of spikes goes to zero and we observe one continuous series of spikes with some height variations. At slightly higher basis fields the spikes become uniform and the oscillation is periodic as shown in Fig. 4(f) for $E_{dc}=6.276$ V/cm.

Figure 5(a) shows an enlarged view of a single-current spike taken from Fig. 4(c). The spike is asymmetric, with a rapid decrease in current followed by a slower recovery. The decrease in current follows from the decrease in electric field in the low-field portion of the sample, which must accompany the formation of a high-field domain in order to keep the voltage drop across the sample constant. The total charge associated with the current pulse is $\approx 5\times 10^{11}$ elementary charges. Figure 5(b) shows a digitized time trace of the periodic current oscillation for an applied bias of $E_{dc}=6.528$ V/cm, plotted with the same scale. The oscillation has a sawtooth shape; each

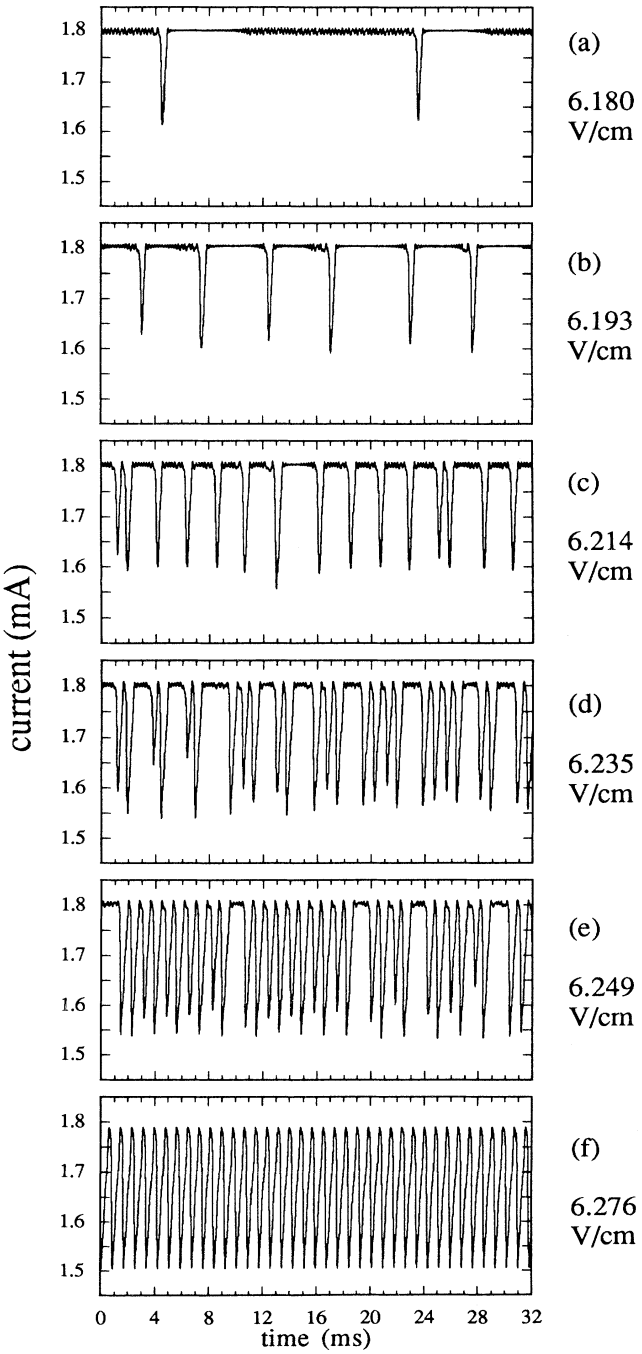

FIG. 4. Time traces of the total sample current for six values of dc bias. The applied bias field E_{dc} indicated at the right increases from (a) to (f).

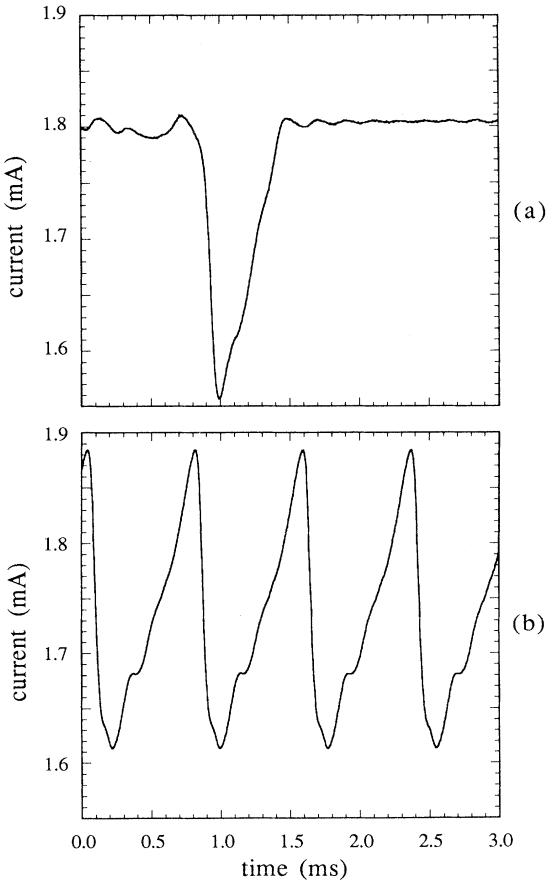

FIG. 5. Time traces of the total sample current with applied bias fields of (a) $E_{dc}=6.214$ V/cm [as in Fig. 4(c)] and (b) $E_{dc}=6.528$ V/cm.

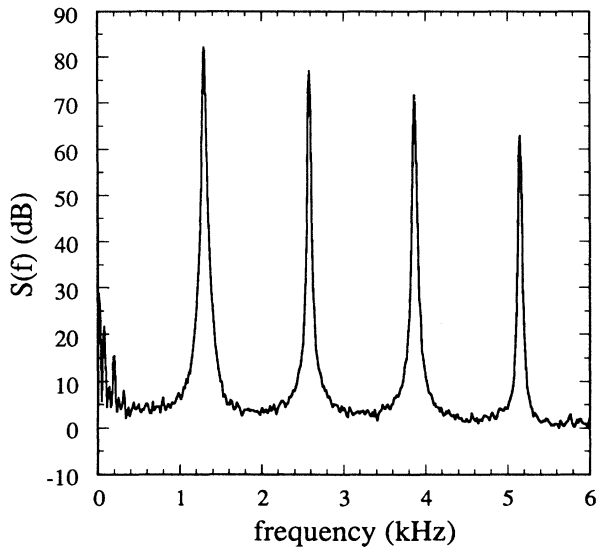

FIG. 6. Power spectrum (in relative units) of the current oscillation with an applied bias of $E_{dc}=6.528$ V/cm [as in Fig. 5(b)] taken using a Hanning window.

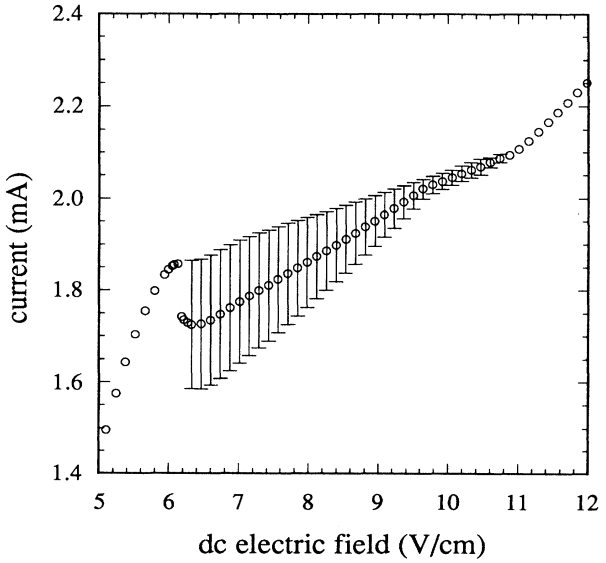

FIG. 8. Time-averaged current vs applied bias field with contact A positive. The bars indicate the peak-to-peak amplitude of the periodic current oscillation.

period of oscillation resembles the single spike shown in Fig. 5(a). The power spectrum of this periodic oscillation, shown in Fig. 6, has a fundamental peak at 1.28 kHz and smaller peaks at harmonics of the fundamental. The oscillation is very clean, having a signal-to-noise ratio greater than 75 dB.

The variation of the oscillation frequency with the applied bias field is shown in Fig. 7. As the bias is increased, the frequency first decreases, reaching a minimum of 1.25 kHz at an applied field of 7 V/cm. As the bias is further increased the frequency increases and the amplitude decreases. A blowup of the region of the I-V curve over which the sample oscillates is shown in Fig. 8. Vertical bars are used to indicate the peak-to-peak amplitude of the current when the oscillation is periodic. This is measured by recording the true rms amplitude and assuming a perfect sawtooth form for the oscillation, which results in a measured peak-to-peak amplitude within 1% of the actual value. The abrupt drop in the time-averaged current at a bias of $E_{dc}=6.2$ V/cm is associated with the onset of current spiking. This abrupt drop is present only for the time-averaged current and not the peak current values because the instability initially occurs as downward current spikes. The first few data points after the drop in current do not have bars because the current spiking is not periodic.

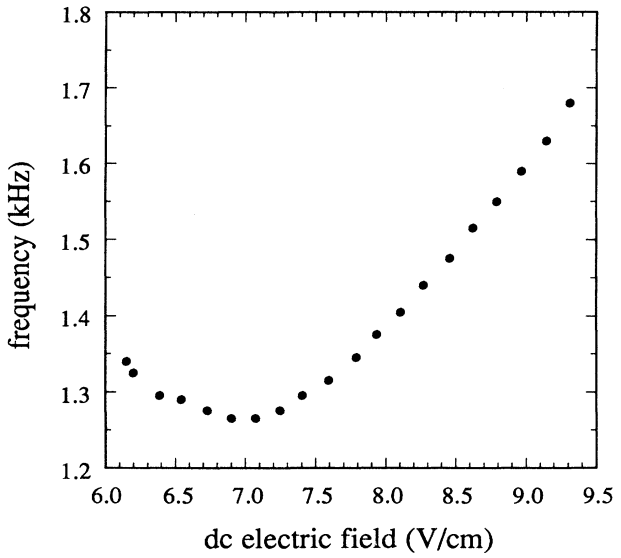

FIG. 7. Frequency of the periodic current oscillation vs applied bias field.

V. SPATIAL MEASUREMENTS WITH dc BIAS

Spatial variations in the local electric field in our samples are constrained by several boundary conditions. The electric field must vanish at both ends of the sample at the Ohmic contacts. In addition, all of our experiments are done with voltage bias, which requires the spatial integral of the electric field to be equal to the applied bias voltage at all times. This boundary condition results in a mechanism for feedback among different parts of the sample since, for dc bias, an increase in the electric field in one region of the sample must be accompanied by a decrease in the average electric field in the rest of the sample.

The spatially dependent sample voltage, measured using the moveable capacitive probe, with the same applied dc bias as in Figs. 5(b) and 6 ($E_{dc}=6.528$ V/cm), is shown in Fig. 9(a). The local sample voltage is plotted as a function of sample position at 12 equally spaced times, 74 μs apart. The injecting contact (A) is on the left of the

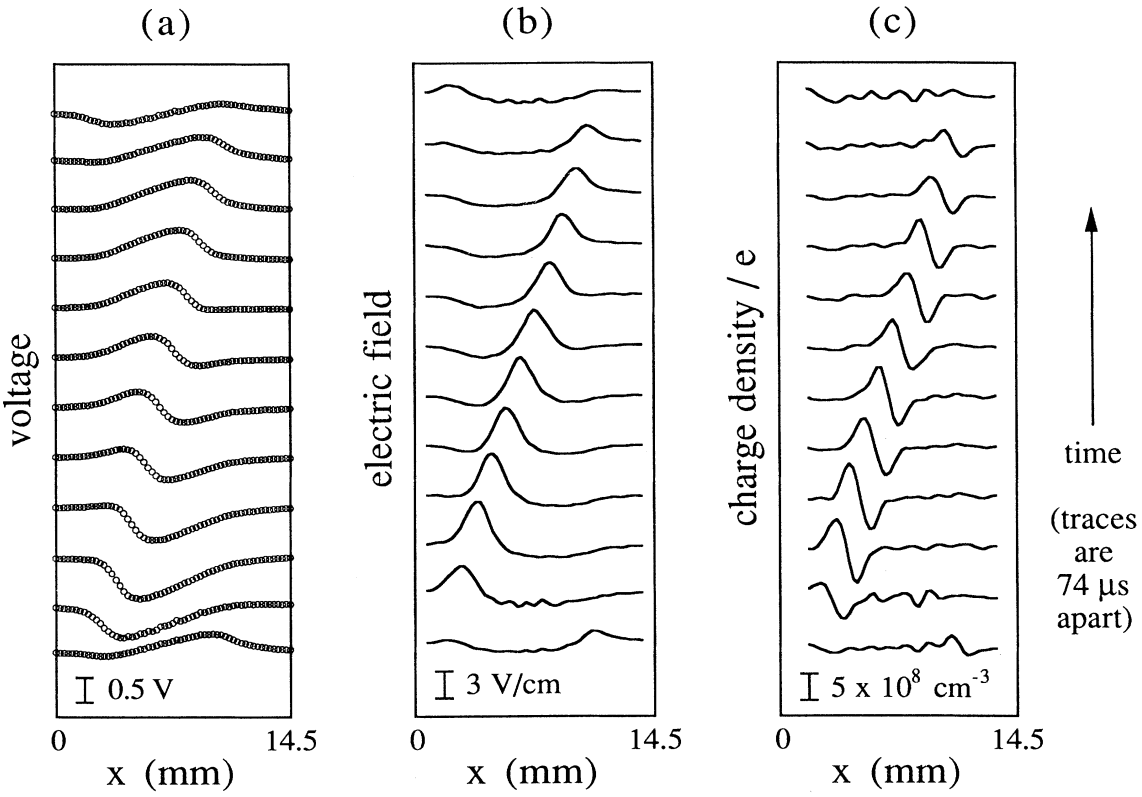

FIG. 9. (a) Local sample voltage vs position x at successive times for slightly more than one period of current oscillation with an applied bias of $E_{dc}=6.528$ V/cm [as in Figs. 5(b) and 6]. The injecting contact (A) is at $x=0$ and the receiving contact (B) is at $x=14.5$ mm. The bottom trace is taken at time $t=0$, as defined by the abscissa in Fig. 5(b). (b) Local electric field vs position, obtained by differentiating the traces in (a). (c) Local charge density vs position obtained by taking the second spatial derivative of the traces in (a).

figure and the bottom trace occurs at time $t=0$ as defined in Fig. 5(b) showing the digitized current. The time between the bottom and the top trace is 814 μs, slightly more than one fundamental oscillation period (781 μs).

Figure 9(b) shows the electric profile of the sample at successive times, obtained by taking spatial derivatives of the data in Fig. 9(a). As shown, a high-field domain forms at the injecting contact and moves smoothly through the sample. The domain is ~ 3 V/cm high and 2 mm wide. As the domain nears the receiving contact, a new domain is nucleated at the injecting contact, and the sequence repeats. The noisy appearance of the field profile while the new domain is forming is due to space-charge fluctuations occurring in the bulk of the sample. As the new domain grows it stabilizes the sample and these other fluctuations are damped out. This stabilizing effect can be understood as follows. As a result of the boundary condition imposed by the fixed dc bias, the growth of the domain is accompanied by a reduction in the local electric field in other parts of the sample. The result is that the wide, flat regions in the electric-field profiles shown in Fig. 9(b) have local electric-field values which are below the threshold for spontaneous current oscillation and fluctuations are damped out. When the domain leaves the sample, the local electric-field values in other parts of the sample increase above the threshold for the instability and space-charge fluctuations result.

A comparison of Fig. 9(b) with Fig. 5(b) shows that the sharp decrease in current is associated with the nucleation of a domain. As the domain moves through the sample the peak value of the electric field decreases [Fig. 9(b)] and the current slowly increases [Fig. 5(b)]. This increase in current accompanying the decrease in domain amplitude follows from the voltage-bias boundary condition: A decrease in domain amplitude must increase the electric field (and current) in the low-field portion of the sample. The current continues to rise as the domain leaves the sample, then abruptly falls when the next domain is nucleated.

The charge density as a function of position is shown in Fig. 9(c). The plots clearly show a dipole layer moving through the sample. The peak-to-peak change in charge density is $\rho/e=1.3\times10^9$ cm^{-3}, which is $\sim 1\%$ of the background shallow acceptor concentration. The total charge associated with one-half of the dipole layer is 8×10^6 elementary charges, much less than the charge associated with one period of the current oscillation.

The position of the peak of the electric-field profile is plotted as a function of time in Fig. 10, showing one fundamental oscillation period, with $t=0$ again defined as in Fig. 5(b). The discreteness of the point spacing occurs because the resolution of the position values is limited by

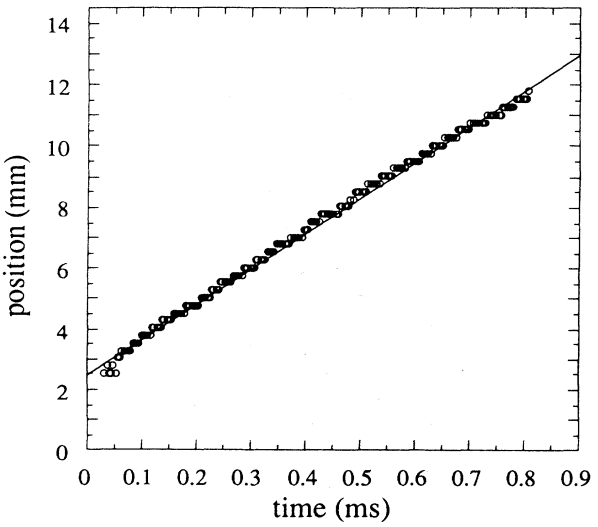

FIG. 10. Location of the maximum value of the local sample electric field vs time with an applied bias of $E_{dc}=6.528$ V/cm [as in Figs. 5(b), 6, and 9]. The data show exactly one period of the fundamental oscillation with time $t=0$ as defined by the abscissa in Fig. 5(b). The straight line is a least-squares fit to the data and corresponds to a domain velocity of 1.16×10^3 cm/s.

the 0.25-mm spacing of the spatial data. The straight line is a least-squares fit to the data, which corresponds to a domain velocity of 1.16×10^3 cm/s. Note that the range of the positions plotted, from $x=2.25$ mm to $x=11.75$ mm, is less than the entire sample length, because a new domain enters the sample before the previous domain has fully exited. The entering domain remains smaller than the exiting domain until the entering domain gets to $x=2.25$ mm, at which point it becomes the larger one. Hence the frequency of oscillation is not given by the domain velocity divided by the sample length, but rather by the domain velocity divided by the distance between domains, which is 9.5 mm in this case. Measurements at several bias fields indicate that the bias dependence of the oscillation frequency is due to variation of both the domain spacing and the domain velocity with the applied bias. The increase in oscillation frequency shown in Fig. 7 above $E_{dc}=7.0$ V/cm is accompanied by a decrease in the domain spacing, which increases the integral of the electric field along the sample.

The observed domain velocity is much slower than the typical free-carrier drift velocity ($\sim10^6$ cm/s) in our samples, implying that these domains are composed of trapped charge in agreement with theoretical models for the instability.[19,20] This is in contrast to domains in Gunn diodes,[23] which move at the drift velocity, resulting in much higher frequency oscillations than we observe. Domain instabilities in doped semiconductors at low temperatures typically move slowly due to the spatial transfer of trapped charge.[1,24]

Theoretical values for the domain velocity and width can be calculated for an infinite sample under current bias using the analysis of Bonilla and Teitsworth[22] by numerically calculating phase-space trajectories and imposing a homoclinicity condition. These values are sensitive to the electric-field dependence of the differential mobility and the impact-ionization cross section. Preliminary calculations[25] using a simplified expression for the differential mobility give widths in agreement with experiment and velocities lower than we observe. Calculations using a more realistic velocity-field relation are in progress.

VI. OTHER SPATIAL MEASUREMENTS

In order to study the spatial structure associated with the spiking of the current which occurs below the threshold for periodic oscillations, we first bias the sample at 4.741 V/cm. This field is beyond the breakdown field but well below the threshold for any current instability. We then apply a step in the applied field to bias the sample within the spiking region, as shown in the plot of the bias wave form in Fig. 11(a). The current response, shown in Fig. 11(b), is a downward spike which occurs immediately after the step in voltage bias. The shape and amplitude resemble those of spontaneous current spikes which occur later at irregular intervals, such as those occurring at times $t=3.6$ ms and $t=4.4$ ms in Fig 11(b).

By triggering our transient recorder just prior to the step in voltage, we can examine the spatial structure of the sample associated with the prompt triggered current spike. The resulting electric field at successive times is shown in Fig. 12. The traces are 98 μs apart with the first trace at $t=0.215$ ms on the time axis of Fig. 11; the voltage step occurs at a time halfway between the first and second trace. Approximately 150 μs after the step, a high-field domain is nucleated at the injecting contact and then moves through the sample, as shown. The

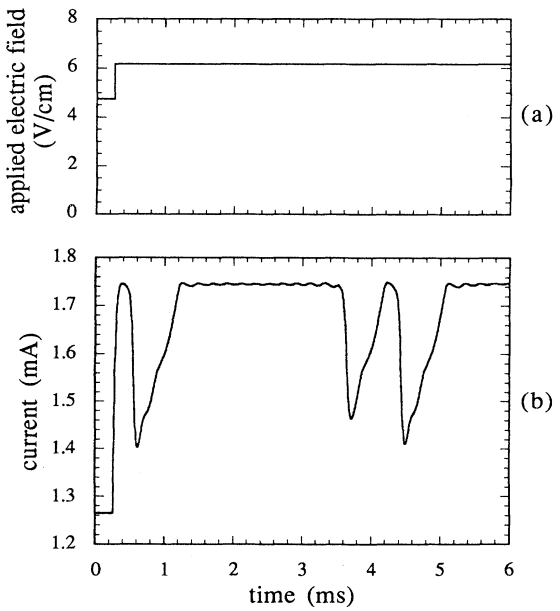

FIG. 11. (a) Applied bias field vs time. (b) Total sample current vs time for the applied bias shown in (a). The time axes are the same in (a) and (b).

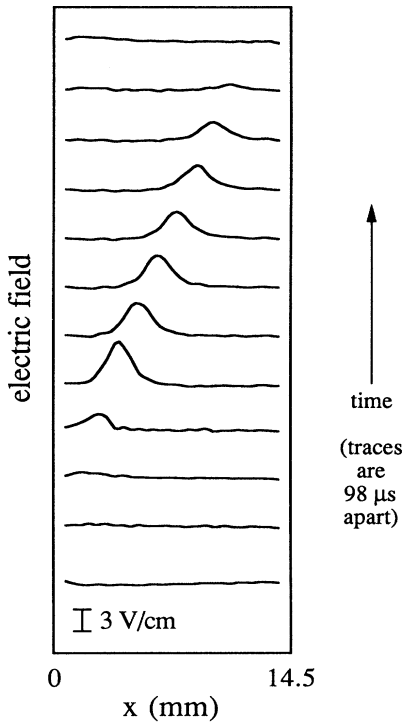

FIG. 12. Local electric field vs position x, for the applied bias field shown in Fig. 11(a). The injecting contact (A) is at $x=0$ and the receiving contact (B) is at $x=14.5$ mm. The bottom trace is taken at time $t=0.215$ ms (just before the step in the applied bias), as defined in Fig. 11.

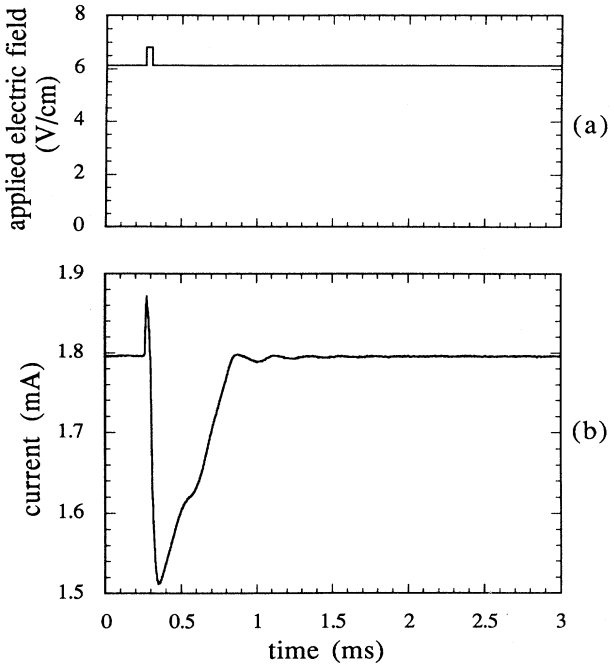

FIG. 13. (a) Applied bias field vs time. (b) Total sample current vs time for the applied bias shown in (a). The time axes are the same in (a) and (b).

prompt current spike in Fig. 11(b) initiates at the same time that the domain is nucleated. The height and shape of the domain are similar to those for the periodic oscillation shown in Fig. 9(b). As the domain in Fig. 12 nears the receiving contact the amplitude decreases, but no new domain is nucleated, unlike the periodic case shown in Fig. 9(b). The last two traces in Fig. 12 show the electric-field profile returning to a spatially uniform state.

Figures 13 and 14 show the response of the sample to a brief square pulse in the applied dc bias. The time-dependent bias is shown in Fig. 13(a). The sample is biased at 6.131 V/cm, just below the onset of the current instability, and the applied pulse is 40 μs wide and 0.662 V/cm high. The current response, shown in Fig. 13(b), has a brief upward rise in current due to the sample capacitance, followed by a large downward spike in current, resembling the spontaneous current spike shown in Figs. 5(a) and the triggered current spike shown in Fig. 11(b). Following the large current spike, there is damped ringing at a frequency ~ 6 kHz. The electric-field profile at successive times is shown in Fig. 14. The first trace is taken prior to the pulse, the second trace is taken at the center of the pulse, and subsequent traces occur after the applied bias has returned to its initial value. As expected, the large downward-current spike is associated with the launching of a high-field domain at the injecting contact. The second trace shows that the rising edge of the bias

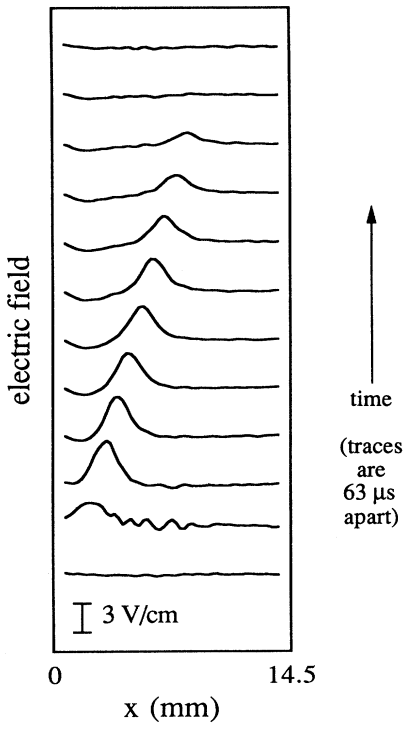

FIG. 14. Local electric field vs position x for the applied bias field shown in Fig. 13(a). The injecting contact (A) is at $x=0$ and the receiving contact (B) is at $x=14.5$ mm. The bottom trace is taken at time $t=0.227$ ms (just before the pulse in the applied bias), as defined in Fig. 13. The second trace is at the center of the square pulse shown in Fig. 13(a) and the third trace is taken after the bias has returned to its initial value.

pulse creates spatial fluctuations in the electric-field profile, which becomes a single high-field domain after the end of the pulse. The domain subsequently grows and moves through the sample. Note that the domain continues to travel long after the sample bias has returned to its initial level, below the threshold of the current instability. In the last traces of Fig. 14 the domain height decreases and the electric-field profile returns to a spatially uniform state.

The presence of a high-field domain is always observed to have a stabilizing effect against other spatial fluctuations in our experiments. We have attempted without success to nucleate a second domain in the sample with a domain already present, by applying a second step or pulse in the sample bias with the dc bias level near the threshold for spontaneous oscillation. The resulting spatial profile either shows small fluctuations that rapidly disappear or the destruction of the original domain and its replacement by a new domain near the injecting contact. As discussed earlier, this stabilizing effect occurs when the formation of a high-field domain decreases the electric field in other parts of the sample.

Figure 15 plots the domain amplitude versus position for both the spontaneous oscillation and domains triggered by pulses for the data in Figs. 9(b) and 14, taken over the entire data sets digitized at 256 kHz. In accord with the boundary conditions imposed by the Ohmic contacts the measured electric fields approach zero near both contacts. In both cases there is a growth region near the injecting contact resulting in a peak domain amplitude of about 5 V/cm one quarter of the way along the sample.

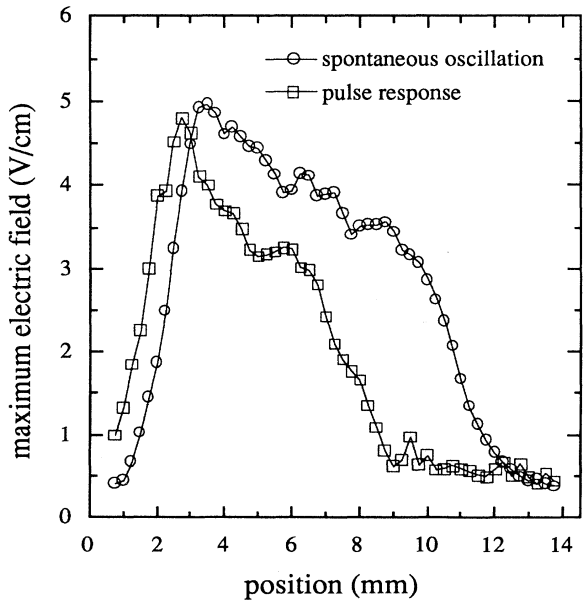

FIG. 15. Maximum electric field at each position. The circles are for the periodic oscillation with an applied dc bias of $E_{dc}=6.528$ V/cm [as in Figs. 5(b), 6, 9, and 10]. The squares are for the response to the pulse shown in Fig. 13(a) [as in Figs. 13(b) and 14]. The lines are drawn as guides.

Beyond this region, the domain amplitudes decrease as the domains approach the receiving contact. As shown, domains triggered by pulses decay more rapidly and die out entirely before they reach the receiving contact.

VII. DISCUSSION AND CONCLUSIONS

These experimental data clearly show that the observed current oscillation in ultrapure Ge is caused by the nucleation and motion of high-electric-field domains due to impact ionization of trapped charge. This is an example of a class of semiconductor systems with interesting spatial dynamics, including Gunn and IMPATT diodes. In these devices the spatial structures are moving high-field domains, which are nonlinear solitary waves. For dc voltage bias different regions of the sample are coupled by the requirement that the integral of the electric field along the sample be equal to the applied voltage.

As the dc voltage bias is increased we observe a transition from dc conduction to periodic current oscillations. This transition occurs via several intermediate steps. First, a small, noisy oscillation occurs with relatively high frequency. Second, large isolated downward-current spikes occur at irregular intervals. Spatial measurements show that each spike is due to the nucleation and subsequent movement of a single domain through the sample. As the bias is increased the spacing between spikes decreases and the spikes occur in increasingly large groups. A third transition occurs when the spacing between groups vanishes, producing a large periodic current oscillation. Each period of the current oscillation is associated with the formation and movement of a high-field domain. The observed domain velocity is much smaller than the carrier drift velocity indicating that the domain is composed of trapped charge.

The shape of current spikes and each cycle of the periodic oscillation can be understood from the position dependence of the domain amplitude shown in Fig. 15. As described above, voltage-bias boundary conditions imply that an increase in high-field domain amplitude must be accompanied by a decrease in field elsewhere in the sample, and thus a decrease in current. The initial sharp decrease in current is due to the rapid formation of a high-field domain, and the slow rise in current is caused by the decay in domain amplitude as it moves through the sample. This decay, shown in Fig. 15, begins far from the receiving contact, where the maximum field is required to approach zero.

When a domain is present in the sample, the nucleation of subsequent domains depends upon the rate of decay of domain amplitude. If the amplitude is sufficiently large when the domain nears the receiving contact, a new domain is nucleated at the injecting contact. Below the bias threshold for spontaneous oscillation we are able to trigger a domain, but the amplitude decays to a negligible value well before reaching the receiving contact, and a new domain is not nucleated. Above threshold the decay rate is slower and each domain succeeds in nucleating another. Hence, for longer samples we expect that the threshold field for spontaneous oscillation would be higher.

Measurements[5,11] of the universal structure of frequency locking were made on samples taken from the same boule of Ge as those reported on here. This earlier work found excellent quantitative agreement between experiment and circle map theory for the power spectrum and for the spectrum of scaling indices $f(\alpha)$. These earlier measurements did not probe the spatial dependence of the current oscillation. In the present work we show that the spatial form of this oscillation consists of high-field domains which periodically traverse the sample. It is interesting that the dynamics of this spatially extended system can be described in the quasiperiodic case by a low-dimensional model, as for certain experiments with fluid systems and with chemical oscillators. We are currently investigating the changes that occur in the spatial pattern of high-field domains when the current is driven chaotic. The measurements will explore the extent to which the system becomes higher dimensional in the chaotic regime through the formation of more complex spatial structures.

ACKNOWLEDGMENTS

We thank S. H. Strogatz and S. W. Teitsworth for helpful discussions. One of us (D.J.M.) acknowledges financial support from AT&T Bell Laboratories. This work was supported in part by the U.S. Office of Naval Research under Grant No. N00014-89-J-1592.

[1]B. K. Ridley and R. G. Pratt, J. Phys. Chem. Solids **26**, 21 (1965).
[2]S. W. Teitsworth, R. M. Westervelt, and E. E. Haller, Phys. Rev. Lett. **51**, 825 (1983).
[3]J. Peinke, A. Mühlbach, R. P. Huebener, and J. Parisi, Phys. Lett. **108A**, 407 (1985).
[4]G. A. Held and C. D. Jeffries, Phys. Rev. Lett. **56**, 1183 (1986).
[5]E. G. Gwinn and R. M. Westervelt, Phys. Rev. Lett. **57**, 1060 (1986); **59**, 247(E) (1987).
[6]K. Aoki and K. Yamamoto, Phys. Lett. **98A**, 72 (1983).
[7]D. G. Seiler, C. L. Littler, R. J. Justice, and P. W. Milonni, Phys. Lett. **108A**, 462 (1985).
[8]Reviewed in E. Schöll, *Nonequilibrium Phase Transitions in Semiconductors* (Springer-Verlag, Berlin, 1987).
[9]K. M. Mayer, R. Gross, J. Parisi, J. Peinke, and R. P. Huebener, Solid State Commun. **63**, 55 (1987).
[10]K. M. Mayer, J. Parisi, and R. P. Huebener, Z. Phys. B **71**, 171 (1988).
[11]E. G. Gwinn and R. M. Westervelt, Phys. Rev. Lett. **59**, 157 (1987).
[12]J. B. Gunn, in *Proceedings of the Symposium on Plasma Effects in Solids, Paris, 1964* (Dunod, Paris, 1965), p. 199.
[13]E. E. Haller, W. L. Hansen, and F. S. Goulding, Adv. Phys. **30**, 93 (1981).
[14]A. M. Kahn, D. J. Mar, and R. M. Westervelt, Solid State Electron. **32**, 1143 (1989).
[15]S. M. Sze, *Physics of Semiconductor Devices,* 2nd ed. (Wiley-Interscience, New York, 1981).
[16]N. M. Haegel (private communication).
[17]R. W. Hamming, *Digital Filters,* 2nd ed. (Prentice-Hall, Englewood Cliffs, NJ, 1983).
[18]R. M. Westervelt and S. W. Teitsworth, J. Appl. Phys. **57**, 5457 (1985).
[19]S. W. Teitsworth, Appl. Phys. A **48**, 127 (1989).
[20]V. V. Mitin, Appl. Phys. A **39**, 123 (1986).
[21]B. K. Ridley, Proc. Phys. Soc. London **82**, 954 (1963).
[22]L. L. Bonilla and S. W. Teitsworth, Physica D (to be published).
[23]Reviewed in P. N. Butcher, Rep. Prog. Phys. **30**, 97 (1967).
[24]B. K. Ridley, J. J. Crisp, and F. Shishiyanu, J. Phys. C **5**, 187 (1972).
[25]S. W. Teitsworth and L. L. Bonilla (private communication).